IEEE Access
Multidisciplinary | Rapid Review | Open Access Journal

Date of publication xxxx 00, 0000, date of current version xxxx 00, 0000.

Digital Object Identifier xxxx

Analogue Radio Over Fiber Aided MIMO Design for the Learning Assisted Adaptive C-RAN Downlink

YICHUAN LI[1], (Student Member, IEEE), K. SATYANARAYANA[1], (Student Member, IEEE), MOHAMMED EL-HAJJAR[1], (Senior Member, IEEE), and LAJOS HANZO[1], (Fellow, IEEE)
[1]NGW Group, School of Electronics and Computer Science, University of Southampton, Southampton SO17 1BJ, U.K.

The financial support of the EPSRC projects EP/Noo4558/1 and EP/L018659/1, as well as of the European Research Council's Advanced Fellow Grant under the Beam-Me-Up project and of the Royal Society's Wolfson Research Merit Award is gratefully acknowledged.

ABSTRACT The cloud/centralised radio access network (C-RAN) architecture is recognised as a strong candidate for the next generation wireless standards, potentially reducing the total cost of ownership. Spatial modulation (SM) is a cost-effective multiple-input-multiple-output (MIMO) solution, where only a single-radio frequency (RF) chain is required for transmission. In this context, we propose analogue radio over fiber (A-RoF) aided MIMO techniques for a learning assisted adaptive C-RAN system, where SM combined with space-time block coding (STBC) is optically processed relying on the optical frequency-indices in the central unit (CU) of the C-RAN, which also is capable of tuning the connected remote radio heads (RRHs). Furthermore, to improve the spectral efficiency, we invoke our proposed flexible C-RAN architecture for implementing learning assisted transceiver adaptation, where the number of RRHs connected to a single user and its modulation techniques employed are controlled using the K-Nearest Neighbour (KNN) algorithm. The simulation results show that the bit error ratio (BER) performance of our A-RoF system is only marginally degraded compared to that operating without the A-RoF link, while benefiting from our energy- and cost-efficient C-RAN design. Moreover, we show that the learning assisted adaptation is capable of outperforming the classic threshold-based adaptation in terms of the system's achievable rate.

INDEX TERMS Analogue Radio Over Fiber, C-RAN, Spatial Modulation, Space-time Block Coding, Fronthaul, Mach-Zehnder Modulator, Transceiver Adaptation, Machine Learning.

NOMENCLATURE

ADC	Analog-to-digital Conversion
AI	Artificial Intelligent
A-RoF	Analogue Radio over Fiber
BER	Bit Error Ratio
BLAST	Bell Laboratories Layered Space-time
BPSK	Binary Phase Shift Keying
BSL	Bit Splitter
CC	Convolutional Coding
CoMP	Coordinated Multi-point
C-RAN	Cloud/Centralised Radio Access Network
CU	Central Unit
DAC	Digital-to-analogue Conversion
DCF	Dispersion-compensating Fiber
DD-MZM	Dual-drive Mach-Zehnder Modulator
EA	Electronic Amplification
EBPF	Electronic Bandpass Filter
EDFA	Erbium-doped Fiber Amplifier
EE	Energy Efficiency
E/O	Electro-to-optic
FBG	Fiber Bragg Grating
ICI	Inter-channel Interference
IoT	Internet of Things
KNN	K-nearest Neighbour
LD	Laser Diode
MIMO	Multiple-input-multiple-output
MINLP	Mixed-integer Non-linear Programming
ML	Maximum Likelihood
MZM	Mach-Zehnder Modulator
OBPF	Optical Bandpass Filter
ODSB	Optical Double Side-band
O/E	Optic-to-electronic
PDF	Probability Density Function
QPSK	Quadrature Phase Shift Keying
RA	Receive Antenna
RF	Radio Frequency

RRH	Remote Radio Head
SE	Spectral Efficiency
SM	Spatial Modulation
SNR	Signal-to-noise Ratio
STC	Space-time Coding
SSMF	Standard Single-mode Fiber
STBC	Space-time Block Coding
STSK	Space-time Shift Keying
TA	Transmit Antenna
V-BLAST	Vertical BLAST
WDM	Wavelength Division Multiplexing

I. INTRODUCTION

Future wireless systems require substantially increased data rates for supporting emerging technologies, such as artificial intelligence (AI) aided driverless vehicles, as well as the growing mobile markets, including the Internet of things (IoT) [1]. These capacity demands require the upgrade of the mobile access networks. The deployment of extra base stations allows serving more users but suffers from more drastically fluctuating inter-channel interference (ICI) [2] in addition to the fact that it significantly increases the cost. Thus, the C-RAN concept [3], [4] has been proposed as a novel mobile architecture revolutionising the functions of conventional base stations. Accordingly, most of the baseband signal processing is migrated to a CU, while the main radio functions of the conventional base station, such as the optic-to-electro (O/E) conversion, amplification, electronic filtering and radio transmission, are migrated to the RRHs, hence resulting in a cost- and power-efficient solution [1], [5], [6]. The novel concept of coordinated multi-point (CoMP) [4], [7] aided communications can also be established with the aid of the C-RAN's centrally controlled processing.

Moreover, by exploiting the fiber's low antenuation, its substantial bandwidth and its immunity to electro-magnetic interference [8], the A-RoF based C-RAN system is capable of simplifying the functions of the RRHs, since both the modulation as well as the analogue-to-digital conversion (ADC) and digital-to-analogue conversion (DAC) operations are carried out by the CU, while the passive optical processing components and antennas used at the RRHs only impose a modest cost [5], [9]. This results in an energy-efficient mobile access network relying on centralised MIMO schemes [10].

The most popular spatial multiplexing technique [11] is the classic Bell laboratories layered space-time (BLAST) scheme, where independent signals are transmitted from independent antennas for improving the spectral efficiency (SE). However, spatial multiplexing aims for imposing the SE without taking into account the overall energy efficiency as well as the complexity. By contrast, SM is characterised by striking an attractive compromise between the SE and energy efficiency (EE), whilst relying on a single-RF chain based solution for multiplexing the classically modulated data and the antenna index based stream [12]. Furthermore, it was shown [12] that at a given SE, the receiver complexity is substantially reduced when compared to the Vertical BLAST (V-BLAST). To elaborate a little further, SM is a low-cost MIMO technique, where only a single one or a small fraction of the transmitter antennas is activated at a time [12]–[15]. Apart from the advantage of relying on a single-RF chain, single-antenna based receiver activating a single antenna results in an ICI-free design [16].

However, SM does not support transmitter-diversity [13], hence this impediment has inspired further research aiming for achieving both multiplexing and diversity gains. For example, Basar *et al.* [17] amalgamated Alamouti's space-time code with the SM, choosing pairs of antennas for Alamouti's STBC transmission, which improved the BER performance of both SM and V-BLAST systems. Furthermore, Sugiura *et al.* [18] proposed the concept of generalised space-time shift keying (STSK) by introducing a dispersion matrix for space-time coding (STC) prior to the SM mapping [19]. As a benefit of the A-RoF schemes' capability of centralising both the digital and radio processing [20], SM-STBC can be implemented centrally in the A-RoF aided C-RANs considered. *In this treatise, we propose an A-RoF aided SM-STBC scheme based on Alamouti code in the C-RAN's CU, which transmits the STBC signal from a pair of wireless transmitters.*

More explicitly, the SM-STBC operations are carried out optically via optical side-band selection, where the drive frequencies and their phase shifts between each arm of the dual-drive Mach-Zehnder modulator (DD-MZM) utilised are mapped to the STBC-activated antenna indices[1], where the switches and the power-thirsty DAC and ADC required in the RRHs for the conventional SM are eliminated, hence realising an energy-efficient A-RoF based C-RAN system relying on an optical processing aided SM-STBC scheme. To elaborate a little further, the STBC signal is directly modulated with the aid of several sets of laser diodes (LDs), and then it is fed into a DD-MZM, where the transmitting optical side-band is selected by the optical index of the drive-frequency and phase-shifters at each STBC symbol period[2]. Then, the modulated signal is carried over standard single-mode fiber (SSMF) and dispersion-compensation fiber (DCF), where the optical signal is passed to an erbium-doped fiber amplifier (EDFA) before being mapped to different antennas by the passive optical components of a wavelength-division-multiplexing demultiplexer (WDM-Demux), fiber Bragg grating (FBG) and then photo-detected to generate the electronic signal. Thus, each SM-STBC signal is processed in the CU using optical indices. We will detail the specifics of this design in Section II.

Note that our proposed scheme adopts the optical single side-band selection philosophy, which has been experimentally verified in our previous A-RoF aided SM study [6]. However, this prototype system only relied on a twin-TA aided SM solution. **This paper addresses the antenna**

[1]For Alamouti's code, a STBC-activated antennas is a pair of antennas for transmitting STBC symbols.

[2]In Alamouti's code, a STBC symbol period refers to two symbol periods.

number-limitation of [6] for enhancing the system performance with the aid of multi-antenna based SM solution, while as a further benefit of our flexible design, we achieve an adaptive C-RAN system using the same A-RoF system. In a nutshell, the concept of [6] is further developed by conceiving an enhanced side-band selection aided SM encoding scheme in this paper, which is capable of supporting any arbitrary number of SM transmitter antennas per RRH.

Moreover, our proposed system is eminently suitable for adapting the number of RRHs supporting a single user, depending on the channel conditions. The number of the RRHs supporting a user can be adjusted by our flexible C-RAN design, where the adaptation is intelligently controlled by the learning-based KNN algorithm. In most of the open literature, transceiver adaptation aims for maximizing the data rate, while guaranteeing an application-specific target BER. Conventional adaptation schemes [21]–[23] tend to compare the estimated SNR experienced to a threshold for determining the most appropriate adaptive configuration to be signalled to the transmitter required for meeting the target-BER requirement. In this context, the popular C-RAN is capable of supporting CoMP [4], [7], where link adaptation [7], [24] using mixed-integer non-linear programming (MINLP) may be invoked for RRH selection [25], [26]. However, hardware imperfections, such as the amplifier non-linearities and the ever-changing wireless channel require an intelligent learning assisted scheme for adaptive transceiver configuration, which is capable of satisfying the target-BER requirements in the face of these time-variant channel-quality fluctuations [27].

Against this backdrop, in this treatise we conceive a bespoke learning-sided solution relying on the classic KNN algorithm for adapting both the number of RRHs supporting a single user and its modulation techniques employed in our proposed C-RAN system.

Thus, the proposed system amalgamates the SM-STBC scheme with A-RoF techniques, hence constituting an adaptive C-RAN system controlled by the KNN algorithm. In a nutshell, the novel contributions of this paper are as follows:

1) We propose an A-RoF aided optical processing based SM-STBC encoding schemes where an optical index constituted by the DD-MZM's drive frequency and their phase shifts eliminates the need for any actively-powered switches, which would be inevitably required by the wireless SM scheme as well as dispensing with the power-thirsty DACs and ADCs in the RRHs.
2) Our system may be readily invoked for adapting the number of RRHs supporting a single user, simply using a laser bank. Furthermore, the proposed adaptive C-RAN system is controlled by a learning-assisted technique, capable of near-instantaneously adapting the number of RRHs as well as the modulation techniques employed. Moreover, the proposed system is capable of achieving a higher data rate than that of the classic threshold-based adaptation.
3) The proposed system concept was inspired by our A-RoF aided twin-antenna SM experimental study of [6]. However, the system advocated in this paper is capable of supporting MIMO techniques having a variable number of antennas by using direct modulation and extra optical indices, where any arbitrary number of transmitter antennas can be supported, while STBC is invoked for the sake of achieving transmit diversity.

The paper is organised as follows. We propose our A-RoF aided C-RAN system model and characterise its BER performance in Section II. Then, we design an adaptive system, where agile transceiver adaptation using the KNN algorithm is employed in Section III, followed by our conclusions in Section IV.

II. PROPOSED A-ROF AIDED C-RAN SYSTEM MODEL

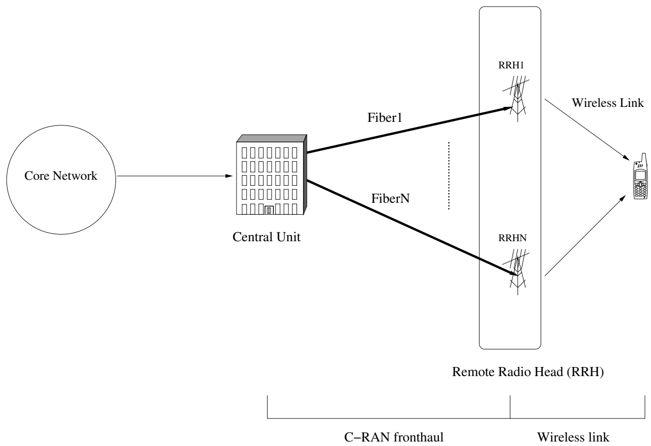

FIGURE 1: An A-RoF aided C-RAN system.

In the context of our C-RAN and MIMO deployment, SM-STBC can be considered a cost-efficient technique of achieving a high throughput and a beneficial diversity gain. To dispense with the power-thirsty antenna switches as well as with the DAC and ADC in the RRHs of the C-RAN system, in this section, we present our A-RoF aided SM-STBC scheme conceived for a C-RAN, where the SM-STBC processing is carried out optically relying on the optical carrier index. Fig. 1 shows a generic fiber-based C-RAN system, where a CU performs most of the signal processing, while the RRHs contain some passive optical components for supporting the associated radio functions.

Let us now consider a C-RAN system, employing our A-ROF aided SM-STBC design shown in Fig. 2, where the schematic of our C-RAN fronthaul design and the wireless link are shown. The proposed system relies on an optical solution for selecting the specific side-band which corresponds to different STBC-activated antennas. This is achieved without employing any actively-powered SM switches and power-thirsty ADCs and DACs. Hence, as shown in Fig. 2, the STBC signal is directly modulated by a set of LDs referred to as a laser bank, resulting in an optical double side-band (ODSB) signal, where each side-band carrying

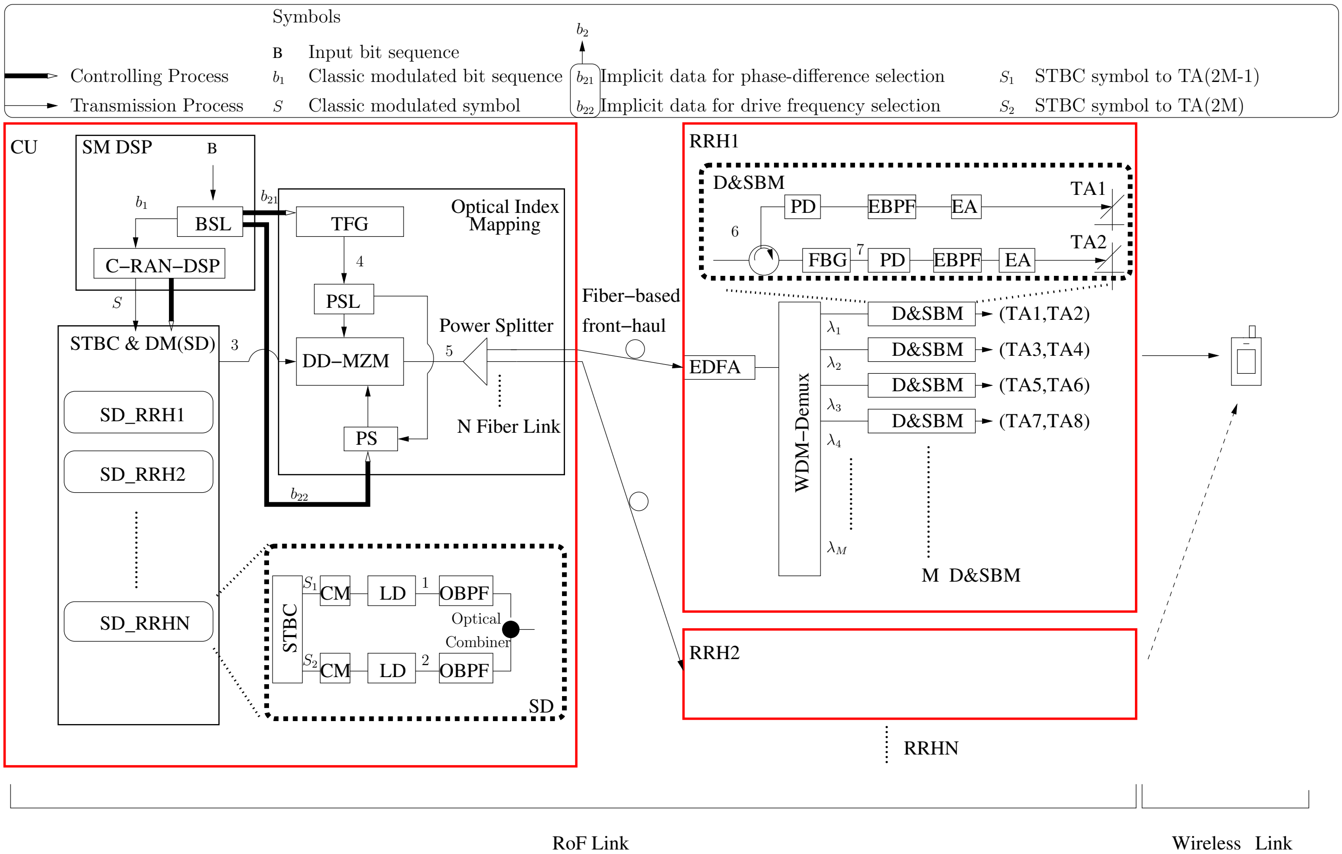

FIGURE 2: Proposed A-RoF aided adaptive C-RAN system.

Alamouti's STBC streams[3] is mapped to each antenna of each RRH. Explicitly, each of the STBC symbols is carried by one of the side-bands of the ODSB-STBC signal, which is then mapped to an antenna at the RRH. Then, with the side-band selection[4] performed by controlling the drive-frequency and the phase shifter of the DD-MZM of Fig. 2, only a single ODSB-STBC signal carrying the Alamouti's code will be transmitted over the fiber at each STBC symbol period, where the side-band selection process would be detailed later in Section II-B. At the fiber receiver of Fig. 2, an EDFA is invoked for optical amplification, while some passive optical components such as a WDM-Demux and FBG are used for side-band to antenna mapping. The WDM-Demux separates each ODSB-STBC signal, and the FBG divides each side-band of the ODSB-STBC signal carrying Alamouti's STBC stream and then passes it on for optic-to-electro (O/E) conversion and electronic amplification (EA). Then, each side-band of the ODSB-STBC signal carrying Alamouti's code is mapped to each STBC-activated antenna of Fig. 2. Note that owing to the side-band selection's capability to transmit a single ODSB-STBC signal at each SM-STBC symbol period, only a pair of the STBC-activated antennas of Fig. 2 would transmit the modulated data during each SM-STBC symbol period, while the remaining antennas remain inactive.

Additionally, we propose an adaptive design, where the number of RRHs supporting a user as well as the modulation technique used per user is adapted. As shown in Fig. 2, the block performing both the STBC scheme and the direct modulation (DM) scheme, where in Fig. 2 we refer to as "STBC & SD (SD)", is capable of adapting the number of connected RRHs by assigning the STBC symbols to each SD_RRHx, hence realising a flexible adaptive C-RAN system, which we will control by invoking a learning algorithm in Section III. This section will only elaborate on our A-RoF aided C-RAN design.

In the proposed design of Fig. 2, the CU performs digital modulation, optical processing aided SM-STBC encoding, radio carrier modulation, electro-to-optic (E/O) conversion and C-RAN RRHs adaptation control, while the RRH implements the associated radio functions (filtering, O/E conversion, photo detection, amplifying and radio transmission), thereby substantially simplifying the transceiver design in the RRH by beneficially centralising the digital processing in the CU.

[3]Here, we refer to the directly modulated ODSB signal carrying the STBC symbols in this stage as the **ODSB-STBC signal** for clarifying our side-band selection process.

[4]To clarify, the "side-band" in this side-band selection refers to a single ODSB-STBC signal generated by direct modulation of Fig. 2, because the ODSB-STBC signal would be viewed as the side-band of an optical carrier after MZM modulation.

A. WIRELESS SM-STBC SCHEME

Prior to discussing our proposed C-RAN design, we will introduce the wireless SM-STBC architecture. SM is a cost-efficient MIMO scheme, where only one of the transmit antennas is activated each symbol period, thus commensurately reducing both the number of RF chains and the ICI. The antenna index and the transmitted symbols are jointly detected at the receiver. In this context, STBC is amalgamated with SM for the sake of attaining a diversity gain. Fig. 3 shows the wireless SM-STBC scheme, where $\mathbf{B}$ is the transmitted input bit sequence, $\hat{\mathbf{B}}$ is the detected bit sequence, N_{TA} is the number of transmit antennas (TAs) and N_r is the number of receive antennas (RAs). In this section, an Alamouti STBC stream is transmitted by activating a pair of the TAs of Fig. 3 during two consecutive symbol periods, jointly forming an STBC symbol period. The statistical SM-STBC model is as follows:

$$\mathbf{Y} = \mathbf{HX} + \mathbf{N}, \tag{1}$$

where $\mathbf{H}$ is the MIMO channel matrix of size $(N_r \times N_{TA})$, $\mathbf{X} = [\mathbf{x_1}, \mathbf{x_2}]$ is the transmitted input SM-STBC matrix of size $N_{TA} \times 2$ with the ith column $\mathbf{x_i}$ denoting the symbol vector transmitted over the ith symbol time of a STBC block[5]. Furthermore, $\mathbf{N} = [\mathbf{n_1}, \mathbf{n_2}]$ denotes the $N_r \times 2$ noise matrix, with the ith column $\mathbf{n_i}$ denoting the receiver noise vector over the ith symbol period of a STBC symbol period. $\mathbf{Y}$ is the received symbol matrix of size $Nr \times 2$, where $\times 2$ denotes two symbol periods. To elaborate a little further, Fig. 4 shows the SM-STBC mapping process, where the input data vector $\mathbf{B}$ is split into two streams, namely b_1 and b_2, where the classic modulated data b_1 is QAM/PSK-modulated for transmission and the antenna selection index b_2 performs the antenna switching to the corresponding TAs [12], [20].

The classic modulated symbols S are transmitted to the corresponding pair of TAs after the STBC processing and radio carrier modulation. For example, if $\mathbf{B} = \{b_1, b_2\} = \{1, 0, 0\}$, we obtain $b_1 = \{1, 0\}$, which is binary phase shift keying (BPSK)-modulated to $S = \{1, -1\}$, while $b_2 = 0$ is used for simultaneously selecting TA1 and TA2 for transmission within a STBC symbol period. Explicitly, after STBC encoding, at the first symbol period, symbol 1 feeds TA1 while -1 feeds TA2. At the second symbol period, symbol -1 feeds TA1 and symbol -1 feeds TA2. Given that at least two RF chains are required to feed a pair of TAs in the proposed SM-STBC scheme, a switch is required to simultaneously control the selected two TAs, enabling the SM-STBC mapping. Following the SM-STBC antenna selection, the vector $\mathbf{X}$ of Equation 1 is denoted by:

[5]Each STBC block utilises two symbol periods and we refer to this as STBC symbol period.

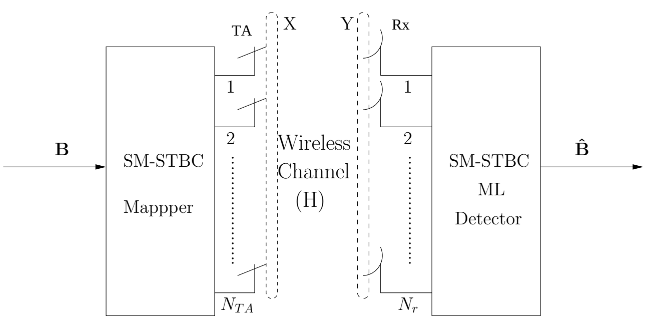

FIGURE 3: Wireless SM-STBC scheme.

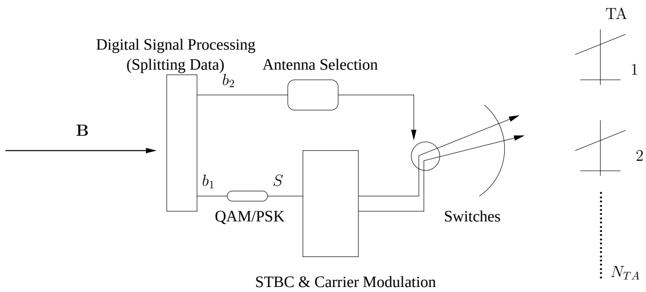

FIGURE 4: Wireless SM-STBC mapper.

$$\begin{bmatrix} 0 & 0 \\ 0 & 0 \\ . & . \\ . & . \\ s_1 & -{s_2}^* \\ s_2 & {s_1}^* \\ 0 & 0 \\ . & . \\ 0 & 0 \end{bmatrix},$$

where

$$\begin{bmatrix} s_1 & -{s_2}^* \\ s_2 & {s_1}^* \end{bmatrix}$$

represents an Alamouti STBC transmitted from the SM-STBC activated-TAs. Furthermore, at the receiver, the classic optimal maximum likelihood (ML) detection [28] is used for jointly detecting both the antenna selection index and the transmitted data.

Based on the above SM-STBC scheme and the C-RAN system, we invoke A-RoF techniques for optically processing the SM-STBC using the optical carrier index mapped to each TA of Fig. 2, where the power-thirsty SM switches, DAC and ADC are eliminated in the RRHs. This concept results in an energy-efficient C-RAN system combined with optical processing aided MIMO signal generation. Next, we will detail the proposed A-RoF aided C-RAN fronthaul design.

B. A-ROF AIDED C-RAN FRONTHAUL DESIGN USING SM-STBC

In this section, we present our system as an energy-efficient and low-complexity mobile fronthaul solution capable of maintaining the BER performance of the above-mentioned wireless SM-STBC scheme.

Fig. 2 shows the schematic of our proposed system design, comprising both a RoF link and a wireless link. In this section we focus our attention on the fiber-based fronthaul design. The SM-STBC encoding process is confined to the CU of Fig. 2, where the ODSB-STBC signal controlled both by the optical index of the phase-shifter and by the drive frequencies of the DD-MZM of Fig. 2 is mapped to each of the activated STBC antennas of Fig. 2. As shown in Fig. 2, the fiber-based fronthaul connects the CU and the RRHs.

To be more explicit, the CU is constituted by three modules, namely the SM scheme's digital signal processing (SM-DSP), the STBC and direct modulation (STBC and DM) and the Optical Index Mapping. At the RRHs, the actively-powered switches used in Section II-A are replaced by a set of passive optical components, which will be detailed later in Section II-B. In the following, we will describe our system based on an eight-TA system per RRH as an example.

1) SM Digital Signal Processing

This module carries out the digital processing operations of SM signal generation, splitting the input bit sequence into index bit sequence for side-band selection and the classic transmitted bit sequence for generating STBC symbols. As shown in Fig. 2, the input bit sequence $\mathbf{B}$ is fed into a bit splitter (BSL) that outputs the pair of bit sequences b_1 and b_2, where b_1 is used for QAM/PSK classic modulation and b_2 controls the optical index of the side-band which corresponds to each TA of the RRH. In our proposed system b_2 is further split into b_{21} and b_{22}. In contrast to the antenna index b_2 of Fig. 4 used in the wireless SM-STBC described in Section II-A, the optical index is related to the phase shift between each arm as well as to the drive frequency of the DD-MZM of Fig. 2, which are controlled by b_{22} and b_{21}, respectively. For example, if we aim for an eight-TA SM-STBC scheme transmitting $\mathbf{B} = \{b_1 = \{0,1\}, b_2 = \{1,1\}\}$, where $\mathbf{B}$ is a binary sequence, b_1 is BPSK-modulated into $S = \{-1,1\}$, which is processed for STBC transmission, while b_2 is further split into $b_{21} = \{1\}$ and $b_{22} = \{1\}$ for the sake of tuning the drive frequency of the tunable frequency generator (TFG) of Fig. 2 and controlling the phase-shifter (PS) of Fig. 2 for ODSB-STBC signal side-band selection corresponding to eight different TAs. Note that the SM-STBC system employing eight antennas will require two bits to select one out of the four possible twin-antenna combinations, hence b_{21} and b_{22} are constituted by a single bit[6]. The C-RAN-DSP of Fig. 2 performs the classic QAM/PSK modulation and centrally processes the data stream transmitted to each RRH using the laser bank in the STBC & DM block of Fig. 2. The mapping rule and its rationale will be discussed in the Paragraphs "**Optical Index Modulation**" and "**Remote Radio Head**" of Sections II-B3 and II-B4.

2) STBC and DM

As shown in Fig. 2, this module consists of a laser bank performing STBC encoding, radio carrier modulation and optical direct modulation. Again, we use an eight-TA SM-STBC scheme as an example for illustration. More specifically, the classic modulated symbol S is assigned to the STBC and DM (SD) block of Fig. 2 for STBC processing[7], where S_1 and S_2 are the STBC symbols transmitted to a pair of STBC-activated TAs of RRH1 of Fig. 2. Then, as shown in Fig. 2, S_1 and S_2 are carried by a RF of frequency f_{RF} via carrier modulation, followed by the LD's direct modulation, whose spectra is shown in Stage 1 and Stage 2 of Fig. 5. The optical bandpass filters (OBPFs) of the SD then retain each side-band containing either S_1 or S_2 to form a new ODSB, as shown in Stage 3 of Fig. 5 using an optical combiner, where S_1 and S_2 are modulated to each side-band of the new ODSB of stage 3 of Fig. 5, where we will refer to the ODSB carrying S_1 and S_2 as ODSB-STBC signal for distinguishing them from our DD-MZM side-band selection process in Section II-B3. Again, the side-band described in the DD-MZM side-band selection can be viewed as a single ODSB-STBC signal, because the ODSB-STBC signal of Stage 3 of Fig. 5 is shifted away from an optical carrier and becomes its side-band, as shown in Stage 5 of Fig. 5. Then, the resultant ODSB of Stage 3 seen in Fig. 5 is fed into the optical index mapping block for side-band selection.

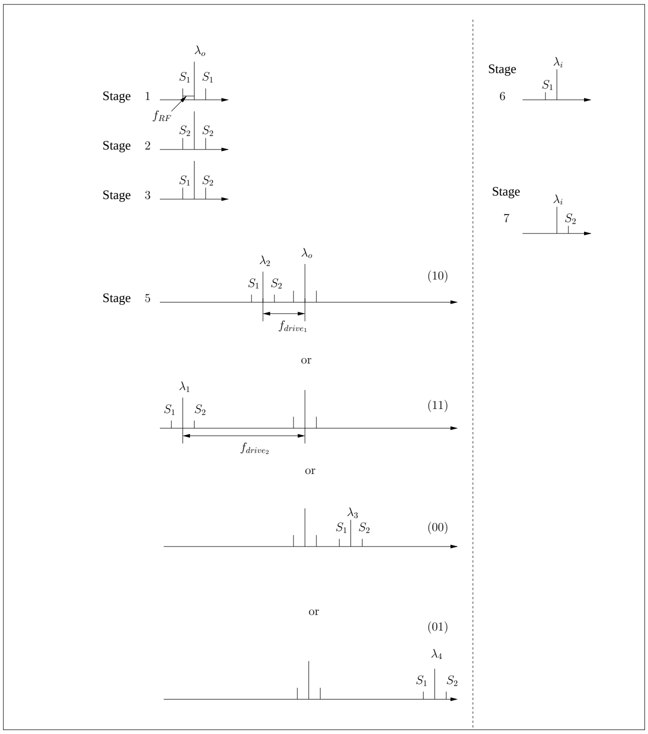

FIGURE 5: Spectrum evolution for 1-RRH scheme (Each stage corresponds to the stage of Fig. 2). Note that Stage 4 of Fig. 2 is not involved here because it only reflects the value of f_{drive}.

[6]For 2M-TA system, b_{21} represents 1-bit information, while b_{22} represents $(\log_2(\mathrm{M}) - 1)$-bit information.

[7]In this example, only single SD module is required for connecting a single RRH. However, the data transmitted to each RRH corresponds to each SD seen in Fig. 2.

TABLE 1: The A-RoF aided eight-TA SM-STBC mapping scheme. Phase Shifting Index, -$\pi/2$ (bit 1); $\pi/2$ (bit 0). Drive Frequency Index, f_{drive_1} (bit 0); f_{drive_2} (bit 1).

Side-band central wavelength	Corresponding TA index	PS index	TFG index
λ_1	(TA1, TA2)	1	1
λ_2	(TA3, TA4)	1	0
λ_3	(TA5, TA6)	0	0
λ_4	(TA7, TA8)	0	1

3) Optical Index Mapping

This module performs the main function of optical index mapping, where the optical index is characterised both by the phase-difference between the drive signal fed into each arm of the DD-MZM and by the DD-MZM's drive frequency, where the locations of the ODSB generated in Stage 3 of Fig. 5 are mapped to different pairs of TAs in Fig. 2. The optical index mapping is mainly performed via changing the phase difference by either $\pi/2$ or $-\pi/2$ between the signal driving the two arms of the DD-MZM and via tuning the drive frequency f_{drive} [29].

Based on our previous experimental feasibility study of the RoF aided twin-antenna SM using side-band selection [6], we are capable of extending our design to any arbitrary number of TAs to support multiple SM schemes. More specifically, the side-band location relies on both the drive frequency controlled by b_{21} and on the phase shifting tuned by b_{22}, as shown in Fig. 2. As verified experimentally and analysed in the literature [6], [29], a phase difference of either $\pi/2$ or -$\pi/2$ between the two drive frequencies of the DD-MZM is capable of moving the ODSB-STBC signal to either the upper side-band or to the lower side-band of the optical carrier of the MZM, while changing the drive frequencies is capable of shifting away the ODSB-STBC signal from the optical carrier of DD-MZM by a frequency spacing of f_{drive}.

Again, considering an eight-TA based SM-STBC scheme, b_{21} is used for controlling the TFG, where the architecture is shown in Fig. 6, shifting the side-band to different frequencies. **The number of controllable drive frequency is linked to the number of SM antennas, where K drive frequencies can be used for mapping the data to $2 \times K_{th}$ pair of STBC transmit antennas, facilitating our arbitrary number of antenna design.** In our system, we use a flexible TFG, which is evolved from our previously proposed TFG of [10]. As shown in Fig. 6, the MZM driven by an unmodulated drive frequency of 15 GHz is invoked for generating a multi-wavelength signal. Following the WDM-Demux and b_{21}-controlled DSP block of Fig. 6 selecting the beating wavelength, the spectra containing λ_a and λ_b is retained and converted to the specific radio frequency of f_{drive}. Explicitly, if the drive signal $f_{drive_1} = 30$ GHz of Fig. 6 is required, given the relationship of $\lambda_b - \lambda_a = \lambda_3 - \lambda_2$, f_{drive} can be flexibly tuned by b_{21}, which results in a tunable frequency generator. Note that tunable commercial microwave generator can also be used in our system. However, we advocate the above-mentioned TFG as a more flexible and low-cost design. On the other hand, during each STBC symbol period, b_{22} flips the PS to either $\pi/2$ or -$\pi/2$ for shifting the ODSB-STBC signal modulated into the optical carrier after the DD-MZM process of Fig. 2 to be either the lower side-band or the upper side-band, as shown in Stage 5 of Fig. 5. The directly modulated ODSB signal of Stage 3 in Fig. 2 feeds a dual-drive MZM for side-band selection driven by a pair of RF signals having a frequency of either f_{drive_1} or f_{drive_2}, as shown in Stage 5 of Fig. 5 selected by b_{21} with a phase-difference of either $\pi/2$ or -$\pi/2$ controlled by b_{22}.

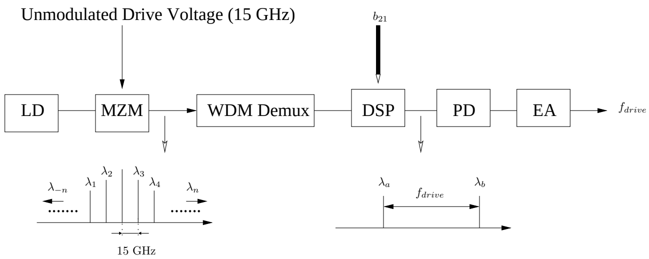

FIGURE 6: Tunable frequency generator.

To clarify the optical index modulation process, for example, as shown in Fig. 2, $(b_{22}, b_{21}) = (1, 0)$ or $(1, 1)$ or $(0, 0)$ or $(0, 1)$ is used for side-band selection, where each combination corresponds to a side-band transmission in a SM-STBC symbol period[8], mapped to (TA1, TA2), (TA3, TA4), (TA5, TA6) and (TA7, TA8) of RRH1 of Fig. 2. The specific mapping rule conceived for an eight-TA SM-STBC system is shown in Table 1. After Stage 5 of Fig. 2, a power splitter is invoked before fiber transmission to serve multiple RRHs, where each fiber strand links the CU to a RRH.

4) Remote Radio Head

As described above, the SM-STBC mapping and digital processing as well as radio carrier modulation are centralised in the CU of Fig. 2. The compact RRHs are responsible for the radio functions such as amplification, O/E conversion, RF filtering and transmission. More explicitly, at the fiber's receiver side, an EDFA is utilised for amplifying the optical signal, followed by a WDM Demultiplexer to filter the corresponding wavelength for the sake of TA mapping. The main components of the side-band to SM-STBC TA mapping operations are shown in the demodulation and side-band mapping (D&SBM) block of Fig. 2. As shown in Fig. 2, we invoke an FBG to separate the side-band of the ODSB-STBC signal obtained in Stage 3 of Fig. 5, which carries the STBC symbols S_1 and S_2. As seen at Stage 6 of Fig.

[8]In Alamouti's code, a SM-STBC symbol period refers to two symbol periods.

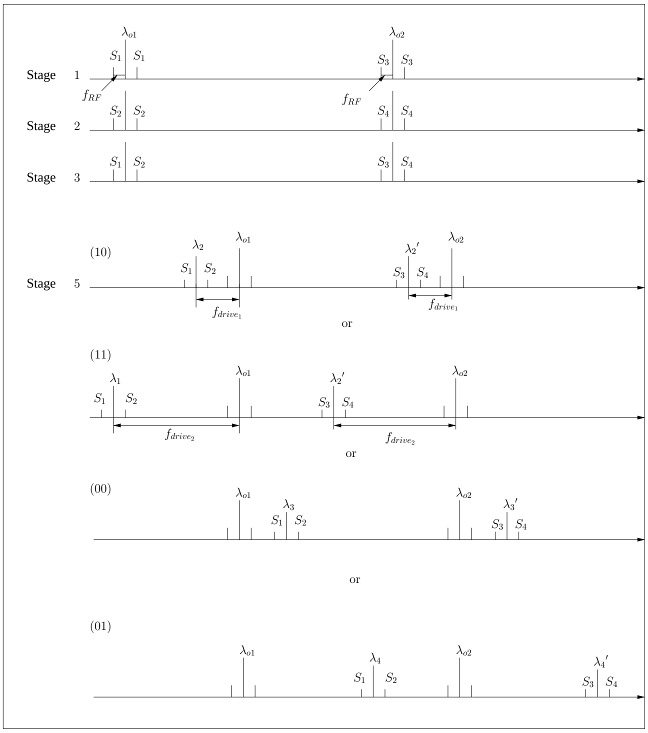

FIGURE 7: Spectrum evolution for 2-RRH scheme (Each stage corresponds to the stage of Fig. 2). Note that Stage 4 of Fig. 2 is not involved here because it only reflects the value of f_{drive}.

5, the lower side-band of λ_i carrying S_1 reflected by the FBG and the upper side-band of λ_i carrying S_2 transmitting through the FBG feed the PDs used for the O/E conversion. Then the resultant signal is passed through an electronic bandpass filter (EBPF) for retaining the desired frequency, followed by an electronic amplifier for boosting the signal to the specific power level required for radio transmission. Lastly, the recovered RF signal f_{RF} carrying S_1 and S_2 is fed into the corresponding pair of TAs, while the remaining inactive antennas radiate negligible low-power noises and the phase noise imposed by the optical and electronic devices.

Fig. 5 shows spectral evolution process of the optical signal. Stages 1, 2 and 3 of Fig. 5 give the direct modulated ODSB, where S_1 and S_2 are carried by the lower side-band and the upper side-band in Stage 3 of Fig. 5. Then, the ODSB signal carrying both S_1 and S_2 feed the Optical Index Mapping module detailed above, where the (b_{22}, b_{21})-selected side-band formed by a single ODSB-STBC signal is transmitted by tuning the frequency of the TFG and PS of Fig. 2 during each SM-STBC symbol period. The mapping rule conceived for the example of an eight-TA scheme is seen at Stage 5 of Fig. 5 and described in Table 1. The fiber-based fronthaul then conveys the optical signal of Stage 5 in Fig. 5 to the RRHs, where a WDM-Demux block transports each side-band to each TA after O/E conversion. Stages 6 and 7 of Fig. 5 show that each optical signal carrying S_1 and S_2 is separated by the FBG, where S_1 and S_2 feed a pair of TAs. Thus, because only a single ODSB-STBC signal carrying the STBC symbols is transmitted during each STBC symbol period, the WDM-Demux of Fig. 2 becomes capable of filtering the specific wavelength in one of the ports, while no data is transmitted from the other ports, hence facilitating the mapping of the side-band index to a specific antenna index using a set of passive optical components.

Furthermore, our system is scalable, where any RRH can be activated by appropriately adjusting the number of activated SD_RRHs of the SD block in Fig. 2. To elaborate a little further, Fig. 7 portrays the spectral evolution, when a CU serves two RRHs. In this scheme, two SD modules, namely SD_RRH1 and SD_RRH2, are assigned the particular sets of STBC symbols S_1, S_2 and S_3, S_4 carried by λ_{o1} and λ_{o2} respectively, where the STBC symbols S_1 and S_2 are transmitted to RRH1, while S_3 and S_4 are forwarded to RRH2. As shown at Stage 5 of Fig. 7, the side-band selection of the two RRHs are consistent, meaning that several RRHs can be jointly controlled merely using a single Optical Index Mapping module. At RRH2, we apply the same architecture, where the WDM de-multiplexed wavelengths are λ_1', λ_2', λ_3' and λ_4'. Hence, a twin-RRH scheme can be readily implemented by adjusting the SD configuration. This configuration inspires our adaptive design, which will be detailed in Section III. Next, our simulation results are presented.

C. SYSTEM SIMULATION

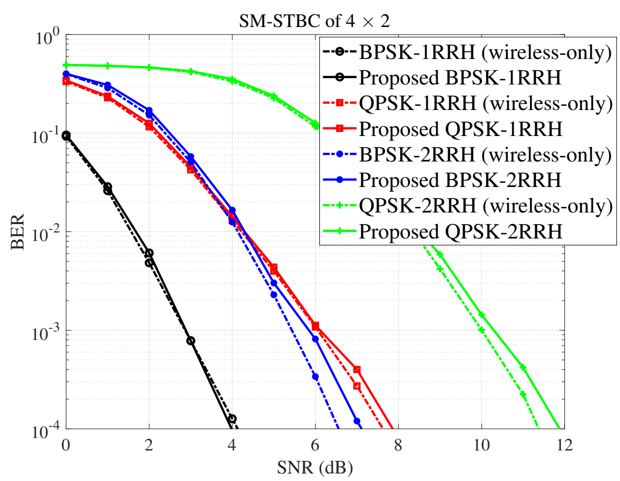

FIGURE 8: BER performance for four TAs and two receive antennas using the schematic of Fig. 2 and parameters of Table 2.

In this section, our simulation results are discussed under two different scenarios. Firstly, we support a user by a single RRH, while relying on an eight-TA SM-STBC scheme. Then, we will increase the number of RRHs, which supports the user, to two, without changing the configuration of the CU as well as the RRHs. Similar to the channel model introduced

TABLE 2: Simulation parameter.

Parameter	Value
Channel coding	Convolutional code
Throughput 4×2	1.5 Gbps (BPSK-1RRH) 2.5 Gbps (BPSK-2RRH) 2.5 Gbps (QPSK-1RRH) 4.5 Gbps (QPSK-2RRH)
Throughput 8×2	2 Gbps (BPSK-1RRH) 3 Gbps (BPSK-2RRH) 3 Gbps (QPSK-1RRH) 5 Gbps (QPSK-2RRH)
LD central wavelength	1550 nm (1 RRH) 1550 nm and 1547.2 nm (2 RRHs: frequency spacing 350 GHz)
RF signal	10 GHz
LD power	1 mW
Drive frequency (MZM)	30 GHz
Fiber type	SSMF+DCF
Fiber length	20 km (15 km SSMF and 5 km DCF)
Channel model	Split-step Fourier method
Modulation type	BPSK and QPSK
Wireless channel	Rayleigh fading channel
Wireless detection	ML detection
Number of TAs	four or eight each RRH
Simulation environment	MATLAB

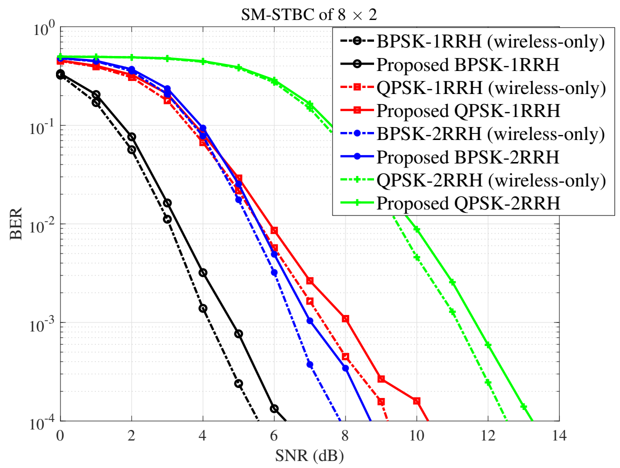

FIGURE 9: BER performance for eight TAs and two receive antennas using the schematic of Fig. 2 and parameters of Table 2.

in Section II-A, the wireless channel is the classic statistical SM-STBC model with A-RoF impairments, as shown below:

$$\mathbf{Y} = \alpha \circ \mathbf{H}\mathbf{X} + \mathbf{N}, \quad (2)$$

where α is the A-RoF-induced distortion[9], and $\mathbf{H}$ is the wireless MIMO channel matrix, both of which have a size of $(N_r \times N_{TA})$. Furthermore, $\circ$ represents the Hadamard product. Here, $\mathbf{H}$ has independent and identically distributed (i.i.d) entries with uniform phase distribution and complex Gaussian distributed amplitude having a mean of 0 and a variance of 1, yielding $\mathcal{CN}$ $\sim$(0,1). $\mathbf{N}$ is the Gaussian noise distributed as $\mathcal{CN}$ $\sim$(0,σ^2). At the wireless receiver, ML detection is used for jointly detecting the antenna index and the classic modulated symbols.

Furthermore, we simulate a SSMF of 15 km and a DCF of 5 km, using the popular split-step Fourier method [30]. The A-RoF parameters used are listed in Table 2. In this section, we consider two scenarios, where single-RRH SM-STBC scheme and two-RRH multiplexing SM-STBC scheme are simulated for the proposed C-RAN system. Explicitly, depending on the specific wireless channel conditions, the user can either communicate by invoking a single RRH using our SM-STBC scheme or with the aid of two RRHs, while multiplexing the signals transmitted from both RRHs, where we use ML detection for both cases. In our proposed A-RoF aided C-RAN shown in Fig. 2, the SD block is used for switching the connection between the single-RRH SM-STBC and two-RRH multiplexing SM-STBC arrangements. For example, if the user is connected to two RRHs, the C-RAN-DSP tends to assign the classic modulated bit sequence b_1 to SD_RRH1 and SD_RRH2 of Fig. 2, thus the signals will be transmitted from both RRH1 and RRH2, multiplexing the SM-STBC signals from each RRH to the same user.

We firstly investigate the SM-STBC scheme using four TAs and two RAs (4×2) schemes, while a pair of TAs transmit the modulated symbols during each STBC symbol period. Moreover, BPSK and quadrature phase shift keying (QPSK) are considered for both the single-RRH SM-STBC and two-RRH multiplexing SM-STBC arrangements. Thus, any of the four configurations shown in Table 2 may be activated by our proposed system. Moreover, the joint throughput after a half-rate convolutional code (CC) is halved. Note that, after the CC process, the modulated symbol rate of the single-RRH scheme is 1 Gsymbol/s[10] while that of the twin-RRH

[9]The distortion is jointly caused by the effects of the A-RoF components, such as fiber's dispersion, fiber's non-linearity, the OBPF's signal leakage and optical noises.

[10]Corresponding bite rate: 1 Gbps for BPSK and 2 Gbps for QPSK.

scheme is 2 Gsymbol/s[11], and the bit rate controlling the optical index is 0.5 Gbps for all the cases. Explicitly, we use a constraint length of 7 and the generator polynomials of (171,133) (in octal), as shown in Table 2 in our proposed system simulation.

To verify that our A-RoF aided system performance is not unduly degraded by the optical link compared to the wireless-only scheme, namely where only wireless transmission relied upon, Fig. 8 shows a modest BER performance of the four configurations, where the scheme operating with A-RoF shows a negligible BER degradation of less than 1 dB compared to that of wireless-only scheme. This modest degradation is imposed by the residual interference introduced by the muted antennas.

Furthermore, our system is eminently scalable. Hence, we also investigate an (8×2) scheme for the sake of increasing the data rate, as seen in Fig. 9 that the BER performance difference between the proposed A-RoF-aided system and the (8×2) wireless-only scheme is higher than that of the (4×2) scheme comparison characterised in Fig. 8. This is because when more antennas are applied, more interference is inflicted, which degrades BER performance.

Next, relying on the system schematic of Fig. 2, we will discuss the benefits of invoking the KNN learning algorithm for transceiver adaptation and compare it to the classic threshold adaptation based benchmarker.

III. LEARNING ASSISTED ADAPTIVE SYSTEM DESIGN

In Section II, we proposed a C-RAN system based on an A-RoF link, where the SM concept is combined with STBC and the signals are processed optically. Furthermore, we discussed that our C-RAN system is scalable of adapting the number of RRHs supporting a user. Similarly, the choice of the modulation technique employed can also be adapted by the SD and C-RAN-DSP module of Fig. 2, depending on the power of the signal received by the user from the RRH.

A. ADAPTATION OF THE PROPOSED C-RAN

To elaborate further, observe in Fig. 2, if a user was served by a single RRH and then the system switches to the twin-RRH mode, the C-RAN-DSP will assign the STBC symbols to SD_RRH1 and SD_RRH2 instead of SD_RRH1 only. Thus, as shown at Stage 3 of Fig. 7, a pair of ODSB-STBC signals are transmitted to the DD-MZM of Fig. 2 for side-band selection, as detailed in Section II. Then the transmitted optical signal is mapped to separate single-mode fibers in order to serve individual RRHs. At the RRH, we invoke the same configuration, except for the demultiplexed wavelengths of the WDM-Demux module, where in the example of Fig. 7, we use $\lambda_1, \lambda_2, \lambda_3, \lambda_4$ at RRH1, while $\lambda'_1, \lambda'_2, \lambda'_3, \lambda'_4$ at RRH2. Thus, our proposed system is capable of supporting multiple RRH connections by adjusting the configuration of the SD block of Fig. 2.

[11]Corresponding bit rate: 2 Gbps for BPSK and 4 Gbps for QPSK.

Hence, we are able to design a system, where the number of RRHs supporting a user can be adapted in order to vary the data rate, while meeting a particular target performance threshold. Hence, we assume the following scenarios:

1) The user is supported by a single-RRH using SM-STBC along with the modulation formats of either BPSK or QPSK.
2) The user is supported by a pair of RRHs transmitting multiplexed signal using SM-STBC using the modulation formats of either BPSK or QPSK.

B. LEARNING MODEL AND RESULTS

We amalgamate our proposed adaptive C-RAN system with a learning technique for improving the achievable data rate of the system, which relies on the classification algorithm. The rationale of the choice behind the KNN algorithm is that most classification algorithms require an explicit functional mapping between the feature set and the classifiers. The feature set in our solution includes the SNR and the BER, while the classifiers are constituted by the number of RRHs connected to a single user, associated with different modulations techniques. Explicitly, for the single RRH case we invoke SM-STBC and for the 2-RRH scenario we invoke SM-STBC and spatial multiplexing. Unfortunately, there is a paucity of information about the functional mapping between the two. Therefore, a KNN classification algorithm is invoked in this section, which removes the need for a functional mapping [31]. The KNN algorithm consists of two stages, namely training and testing. During the training phase, the samples containing the information, such as the instantaneous SNR and its corresponding BER, is collected over different channel realisations. Then, in the testing phase, we have to decide about the class that is to be employed for attaining a high data rate as well as meeting the target BER. The BER vs SNR relationship may be observed in the stylized illustration of Fig. 10, where depending on the prevalent SNR, we select the transceiver mode capable of satisfying the BER requirement.

The conventional threshold adaptation relies on the BER vs SNR relationship and the SNR values meeting the target BER. For example, let us consider the results of Fig. 9. Assuming that the target at BER$= 10^{-3}$ defines SNRs, the points of intersection of the horizontal line at the BER of 10^{-3}, where the transmission mode reconfiguration has to take place [23]. By contrast, the KNN classification relies on the training data. For example, as shown in Fig. 10, we aim for switching between Configuration 1 and Configuration 2, which are represented by squares $\square$ and triangles $\triangle$. The testing point of Fig. 10 is the centroid used for representing the symbols encircled, which determines the specific configuration activated. Compared to the conventional adaptation relying on a threshold adaptation, the KNN classification assisted adaptation achieves a higher throughput.

As mentioned in Section II, our RoF aided SM-STBC is capable of flexibly switching between the single-RRH and

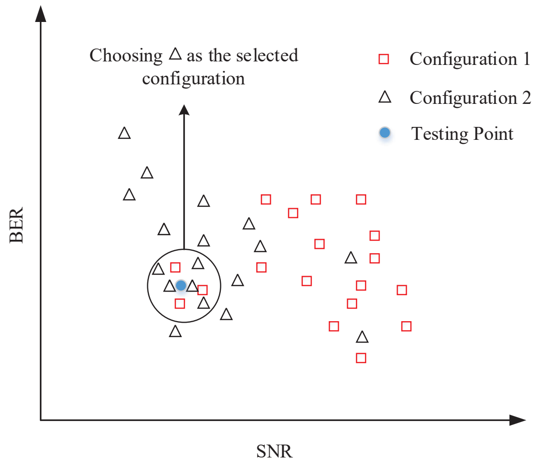

FIGURE 10: Stylized portrayal of the KNN algorithm.

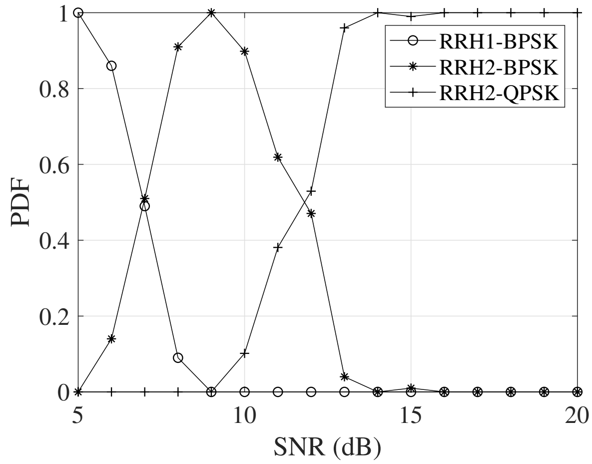

FIGURE 12: Probability distribution function after KNN algorithm using the schematic of Fig. 2 and parameters of Table 2.

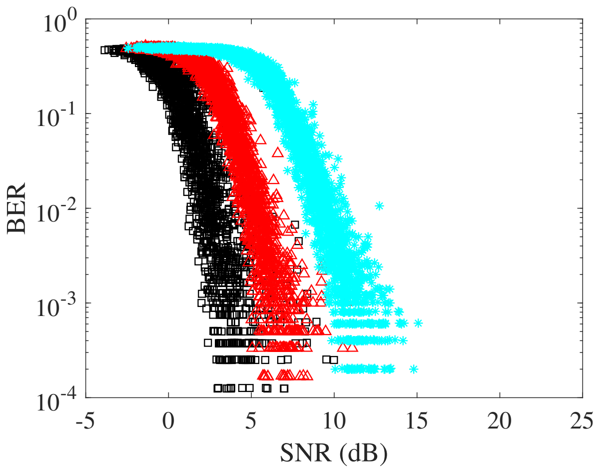

FIGURE 11: Stored training data.

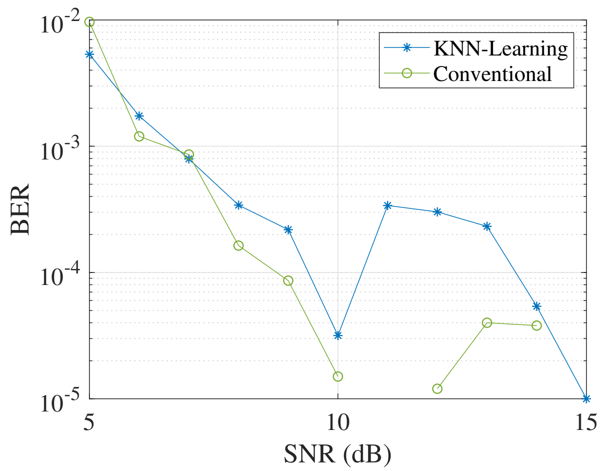

FIGURE 13: BER comparison between KNN algorithm aided adaptation and the conventional adaptation using the schematic of Fig. 2 and parameters of Table 2.

twin-RRHs aided configuration, thus under the control of the KNN algorithm.

As discussed in Section II, given our fixed symbol rate, which corresponds to a fixed maximum RF modulated bandwidth, the BER performance of the BPSK-2RRH scheme becomes slightly better than that of QPSK-1RRH. Thus, we consider the following three configurations or classes for our adaptation technique based on the SM-STBC scheme (8×2) to verify the feasibility of controlling our adaptive C-RAN system by the KNN algorithm, while employing a convolutional code having a code rate of $1/2$, a constraint length of 7 and generator polynomials of (171,133) (in octal). The following are the three configurations used in our adaptive system:

1) 2 Gbps BPSK-1RRH;
2) 3 Gbps BPSK-2RRH;
3) 5 Gbps QPSK-2RRH;

Again, the simulations rely on the training phase and the testing phase. In the training phase, we store the training data associated with the pair of features $\{BER, SNR\}$, namely the BER and the instantaneous post-processing SNR for each channel realisation associated with a different noise level. Hence, in our system, we store 300 training symbols for each of the 20 noise levels considered. Fig. 11 shows the training data stored for the above-mentioned scenarios, where the squares, triangles and stars denote schemes representing the BPSK-1RRH, BPSK-1RRH and QPSK-2RRH schemes, respectively. The target BER of our system is 10^{-3} and the testing point is $\{10^{-3}, M\}$, where M denotes the real instantaneous post-processing SNR.

Thus, we compare the total number of each class encircled and determine which class (configuration) is used for that

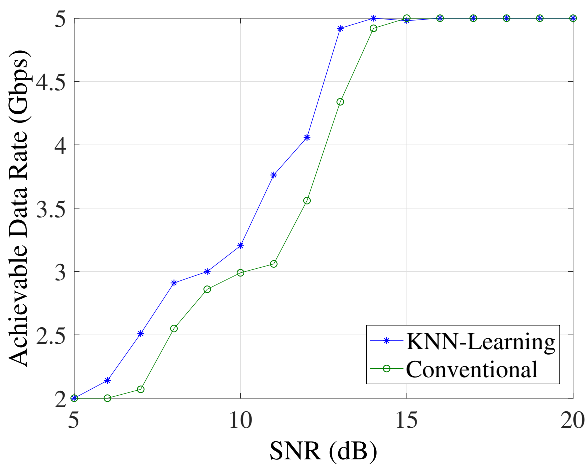

FIGURE 14: Data rate comparison between KNN algorithm aided adaptation and the conventional adaptation using the schematic of Fig. 2 and parameters of Table 2.

specific time slot. We performed Monte-Carlo simulations, where 100 frames each containing 8000 bits were used for each instantaneous post-processing SNR. Then, we obtained the probability density function (PDF) of the three classes tested, which is seen in Fig. 12. For example, around 7 dB around, we have a similar probability of choosing RRH1-BPSK and RRH2-BPSK. Upon increasing the SNR, the probability of the RRH1-BPSK mode is increased, while that of the RRH2-BPSK mode tends to zero upon approaching 9 dB. Then, the RRH2-QPSK mode shows increasingly high probability beyond 9 dB, while at 16 dB, the RRH2-BPSK probability tends to zero.

Fig. 13 shows that our KNN-learning algorithm is indeed capable of maintaining a BER below 10^{-3}. Compared to the classic threshold based adaptation [23], we show in Fig. 14 that the KNN assisted user adaptation improves the achievable data rate. Although, we observe in Fig. 13 that the BER performance of the conventional threshold adaptation is superior to that of our KNN-assisted solution, both techniques are capable of attaining target BER performance. Explicitly, the KNN-based learning algorithm achieves a higher throughput, because it does not maintain an unnecessarily low BER- it rather encourages the activation of higher-throughput modes.

IV. CONCLUSION

In this paper, we proposed an A-RoF aided SM-STBC scheme using optical side-band selection and further extended it to an adaptive C-RAN system, where any arbitrary number of transmitter antennas can be driven by a single MZM. In our proposed system, the power thirsty ADC, DAC and the active-powered switches of a conventional system are eliminated, resulting in an energy-efficient and cost-efficient mobile access network, where the BER performance of this A-RoF aided solution is only marginally degraded compared to the conventional wireless SM-STBC scheme. Moreover, by taking advantage of the flexibly selectable number of RRHs of the proposed A-RoF aided C-RAN system, we invoked the KNN algorithm for intelligently adapting both the number of selected RRHs and the modulation format, showing that the achievable data rate exceeded that of the classic threshold adaptation.

• • •

REFERENCES

[1] L. Hanzo, H. Haas, S. Imre, D. O'Brien, M. Rupp, and L. Gyongyosi, "Wireless myths, realities, and futures: From 3G/4G to optical and quantum wireless," Proceedings of the IEEE, vol. 100, pp. 1853–1888, May 2012.

[2] A. Goldsmith, Wireless communications. Cambridge university press, 2005.

[3] M. Peng, K. Zhang, J. Jiang, J. Wang, and W. Wang, "Energy-efficient resource assignment and power allocation in heterogeneous cloud radio access networks," IEEE Transactions on Vehicular Technology, vol. 64, pp. 5275–5287, Nov. 2015.

[4] A. Checko, H. L. Christiansen, Y. Yan, L. Scolari, G. Kardaras, M. S. Berger, and L. Dittmann, "Cloud RAN for mobile networks—–a technology overview," IEEE Communications Surveys Tutorials, vol. 17, pp. 405–426, First Quarter 2015.

[5] C. Liu, L. Zhang, M. Zhu, J. Wang, L. Cheng, and G. K. Chang, "A novel multi-service small-cell cloud radio access network for mobile backhaul and computing based on radio-over-fiber technologies," Journal of Lightwave Technology, vol. 31, pp. 2869–2875, Sept. 2013.

[6] Y. Li, Q. Yang, I. A. Hemadeh, M. El-Hajjar, C.-K. Chan, and L. Hanzo, "Experimental characterization of the radio over fiber aided twin-antenna spatial modulation downlink," Optics Express, vol. 26, pp. 12432–12440, May 2018.

[7] R. Irmer, H. Droste, P. Marsch, M. Grieger, G. Fettweis, S. Brueck, H. P. Mayer, L. Thiele, and V. Jungnickel, "Coordinated multipoint: Concepts, performance, and field trial results," IEEE Communications Magazine, vol. 49, pp. 102–111, Feb. 2011.

[8] V. Thomas, M. El-Hajjar, and L. Hanzo, "Performance improvement and cost reduction techniques for radio over fiber communications," IEEE Communications Surveys Tutorials, vol. 17, pp. 627–670, Second Quarter 2015.

[9] D. Novak, R. B. Waterhouse, A. Nirmalathas, C. Lim, P. A. Gamage, T. R. Clark, M. L. Dennis, and J. A. Nanzer, "Radio-over-fiber technologies for emerging wireless systems," IEEE Journal of Quantum Electronics, vol. 52, pp. 1–11, Jan. 2016.

[10] Y. Li, M. El-Hajjar, and L. Hanzo, "Joint space-time block-coding and beamforming for the multiuser radio over plastic fiber downlink," IEEE Transactions on Vehicular Technology, vol. 67, pp. 2781–2786, March 2018.

[11] N. Ishikawa, S. Sugiura, and L. Hanzo, "50 years of permutation, spatial and index modulation: From classic RF to visible light communications and data storage," IEEE Communications Surveys Tutorials, vol. 20, pp. 1905–1938, Third Quarter 2018.

[12] R. Y. Mesleh, H. Haas, S. Sinanovic, C. W. Ahn, and S. Yun, "Spatial modulation," IEEE Transactions on Vehicular Technology, vol. 57, pp. 2228–2241, July 2008.

[13] M. D. Renzo, H. Haas, A. Ghrayeb, S. Sugiura, and L. Hanzo, "Spatial modulation for generalized MIMO: Challenges, opportunities, and implementation," Proceedings of the IEEE, vol. 102, pp. 56–103, Jan. 2014.

[14] I. A. Hemadeh, M. El-Hajjar, S. Won, and L. Hanzo, "Multi-set space-time shift-keying with reduced detection complexity," IEEE Access, vol. 4, pp. 4234–4246, June 2016.

[15] Y. Chen, L. Wang, Y. Ai, B. Jiao, and L. Hanzo, "Performance analysis of NOMA-SM in vehicle-to-vehicle massive MIMO channels," IEEE Journal on Selected Areas in Communications, vol. 35, pp. 2653–2666, Dec. 2017.

[16] C. X. Wang, F. Haider, X. Gao, X. H. You, Y. Yang, D. Yuan, H. M. Aggoune, H. Haas, S. Fletcher, and E. Hepsaydir, "Cellular architecture and key technologies for 5G wireless communication networks," IEEE Communications Magazine, vol. 52, pp. 122–130, Feb. 2014.

[17] E. Basar, U. Aygolu, E. Panayirci, and H. V. Poor, "Space-time block coded spatial modulation," IEEE Transactions on Communications, vol. 59, pp. 823–832, March 2011.

[18] S. Sugiura, S. Chen, and L. Hanzo, “Generalized space-time shift keying designed for flexible diversity-, multiplexing- and complexity-tradeoffs,” IEEE Transactions on Wireless Communications, vol. 10, pp. 1144–1153, April 2011.

[19] S. Sugiura, S. Chen, and L. Hanzo, “A universal space-time architecture for multiple-antenna aided systems,” IEEE Communications Surveys Tutorials, vol. 14, pp. 401–420, Second Quarter 2012.

[20] Y. Li, I. A. Hemadeh, M. El-Hajjar, and L. Hanzo, “Radio over fiber downlink design for spatial modulation and multi-set space-time shift-keying,” IEEE Access, vol. 6, pp. 21812–21827, March 2018.

[21] T. L. Jensen, S. Kant, J. Wehinger, and B. H. Fleury, “Fast link adaptation for MIMO OFDM,” IEEE Transactions on Vehicular Technology, vol. 59, pp. 3766–3778, Oct. 2010.

[22] L. Chen, Y. Yang, X. Chen, and G. Wei, “Energy-efficient link adaptation on Rayleigh fading channel for OSTBC MIMO system with imperfect CSIT,” IEEE Transactions on Vehicular Technology, vol. 62, pp. 1577–1585, May 2013.

[23] M. El-Hajjar, S. Zummo, and L. Hanzo, “Near-instantaneously adaptive cooperative uplink schemes based on space-time block codes and V-Blast,” in 2007 IEEE 65th Vehicular Technology Conference - VTC2007-Spring, pp. 2200–2204, April 2007.

[24] K. Satyanarayana, M. El-Hajjar, P. H. Kuo, A. Mourad, and L. Hanzo, “Adaptive transceiver design for C-RAN in mmwave communications,” IEEE Access, vol. PP, pp. 1–1, Nov. 2017.

[25] J. Tang, W. P. Tay, and T. Q. S. Quek, “Cross-layer resource allocation with elastic service scaling in cloud radio access network,” IEEE Transactions on Wireless Communications, vol. 14, pp. 5068–5081, Sept. 2015.

[26] Y. Cheng, M. Pesavento, and A. Philipp, “Joint network optimization and downlink beamforming for CoMP transmissions using mixed integer conic programming,” IEEE Transactions on Signal Processing, vol. 61, pp. 3972–3987, Aug. 2013.

[27] R. C. Daniels, C. M. Caramanis, and R. W. Heath, “Adaptation in convolutionally coded MIMO-OFDM wireless systems through supervised learning and SNR ordering,” IEEE Transactions on Vehicular Technology, vol. 59, pp. 114–126, Jan. 2010.

[28] J. Jeganathan, A. Ghrayeb, and L. Szczecinski, “Spatial modulation: optimal detection and performance analysis,” IEEE Communications Letters, vol. 12, pp. 545–547, Aug. 2008.

[29] G. Smith, D. Novak, and Z. Ahmed, “Technique for optical SSB generation to overcome dispersion penalties in fibre-radio systems,” Electronics Letters, vol. 33, pp. 74–75, Jan. 1997.

[30] G. P. Agrawal, Nonlinear fiber optics. Academic press, 2007.

[31] R. O. Duda and P. E. Hart, “Pattern classification and scene analysis,” A Wiley-Interscience Publication, New York: Wiley, 1973.

YICHUAN LI received B.Sc. degree in Optics Information Science and Technology from China University of Petroleum (East China), Qingdao, China, in 2012, and M.Sc. degree in wireless communications from the University of Southampton, Southampton, UK., in 2014. He was a research assistant in the Lightwave Communication Lab of the Chinese University of Hong Kong (CUHK) from July to October in 2017. Currently, he is working toward the Ph.D. degree with the University of Southampton. His research is focused on the the radio over fiber for backhaul, fronthaul and indoor communication network. His research interests are millimeter wave over fiber, optical fiber aided analogue beamforming techniques, Multifunctional MIMO, mode division multiplexing in multimode fiber and fiber-based C-RAN system.

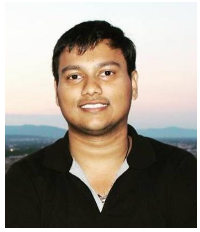

KATLA SATYANARAYANA received his B. Tech. degree in Electrical Engineering from Indian Institute of Technology Madras, India, in 2014. During Jul’14-Aug’15, he worked as a research assistant at Indian Institute of Science, Bangalore. Currently, Satya is a research scholar in Wireless Communications at the University of Southampton in liaison with InterDigital Europe, London, UK. His research interests include millimeter wave communications, hybrid beamforming, with an emphasis on transceiver algorithms for wireless communication systems and multi-functional MIMO.

MOHAMMED EL-HAJJAR is an Associate Professor in the Department of Electronics and Computer Science in the University of Southampton. He received his PhD in Wireless Communications from the University of Southampton, UK in 2008. Following the PhD, he joined Imagination Technologies as a design engineer, where he worked on designing and developing Imagination’s multi-standard communications platform, which resulted in three patents. He is the recipient of several academic awards and has published a Wiley-IEEE book and in excess of 80 journal and conference papers. Mohammed’s research interests include the development of intelligent communications systems, energy-efficient transceiver design, MIMO, millimeter wave communications, machine learning for wireless communications and and Radio over fiber network design.

LAJOS HANZO FREng, FIEEE, FIET, Fellow of EURASIP, DSc received his degree in electronics in 1976 and his doctorate in 1983. In 2009 he was awarded an honorary doctorate by the Technical University of Budapest and in 2015 by the University of Edinburgh. In 2016 he was admitted to the Hungarian Academy of Science. During his 40-year career in telecommunications he has held various research and academic posts in Hungary, Germany and the UK. Since 1986 he has been with the School of Electronics and Computer Science, University of Southampton, UK, where he holds the chair in telecommunications. He has successfully supervised 112 PhD students, co-authored 18 John Wiley/IEEE Press books on mobile radio communications totalling in excess of 10 000 pages, published 1800+ research contributions at IEEE Xplore, acted both as TPC and General Chair of IEEE conferences, presented keynote lectures and has been awarded a number of distinctions. Currently he is directing a 60-strong academic research team, working on a range of research projects in the field of wireless multimedia communications sponsored by industry, the Engineering and Physical Sciences Research Council (EPSRC) UK, the European Research Council’s Advanced Fellow Grant and the Royal Society’s Wolfson Research Merit Award. He is an enthusiastic supporter of industrial and academic liaison and he offers a range of industrial courses. He is also a Governor of the IEEE VTS. During 2008 - 2012 he was the Editor-in-Chief of the IEEE Press and a Chaired Professor also at Tsinghua University, Beijing. For further information on research in progress and associated publications please refer to http://www-mobile.ecs.soton.ac.uk